Journal of Environmental Radioactivity 250 (2022) 106905

Contents lists available at ScienceDirect

Journal of Environmental Radioactivity

journal homepage: www.elsevier.com/locate/jenvrad

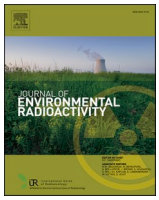

Gas diffusion through variably-water-saturated zeolitic tuff: Implications for transport following a subsurface nuclear event

Chelsea W. Neil [a,*], Hakim Boukhalfa [a], Hongwu Xu [a], S. Douglas Ware [a], John Ortiz [a,b], Sofia Avendaño [a,#], Dylan Harp [a,1], Scott Broome [c], Rex P. Hjelm [d], Yimin Mao [e,f], Robert Roback [a], William P. Brug [a], Philip H. Stauffer [a]

[a] Earth and Environmental Sciences Division, Los Alamos National Laboratory, Los Alamos, NM, 87545, USA
[b] Department of Environmental Health and Engineering, The Johns Hopkins University, Baltimore, MD, 21218, USA
[c] Sandia National Laboratories, Albuquerque, NM, 87185, USA
[d] National Security Education Center, Los Alamos National Laboratory and the New Mexico Consortium, Los Alamos, NM, 87545, USA
[e] Department of Materials Science and Engineering, University of Maryland, College Park, MD, 20742, USA
[f] NIST Center for Neutron Research, National Institute of Standards and Technology, Gaithersburg, MD, 20899, USA

ARTICLE INFO

Keywords:
Underground nuclear explosion
Diffusion
Zeolites
Nonproliferation
Noble gases

ABSTRACT

Noble gas transport through geologic media has important applications in the characterization of underground nuclear explosions (UNEs). Without accurate transport models, it is nearly impossible to distinguish between xenon signatures originating from civilian nuclear facilities and UNEs. Understanding xenon transport time through the earth is a key parameter for interpreting measured xenon isotopic ratios. One of the most challenging aspects of modeling gas transport time is accounting for the effect of variable water saturation of geological media. In this study, we utilize bench-scale laboratory experiments to characterize the diffusion of krypton, xenon, and sulfur hexafluoride (SF_6) through intact zeolitic tuff under different saturations. We demonstrate that the water in rock cores with low partial saturation dramatically affects xenon transport time compared to that of krypton and SF_6 by blocking sites in zeolitic tuff that preferentially adsorb xenon. This leads to breakthrough trends that are strongly influenced by the degree of the rock saturation. Xenon is especially susceptible to this phenomenon, a finding that is crucial to incorporate in subsurface gas transport models used for nuclear event identification. We also find that the breakthrough of SF_6 diverges significantly from that of noble gases within our system. When developing field scale models, it is important to understand how the behavior of xenon deviates from chemical tracers used in the field, such as SF_6 (Carrigan et al., 1996). These new insights demonstrate the critical need to consider the interplay between rock saturation and fission product sorption during transport modeling, and the importance of evaluating specific interactions between geomedia and gases of interest, which may differ from geomedia interactions with chemical tracers.

1. Introduction

Gas transport through rock has important implications for the detection of underground clandestine nuclear tests (Auer et al., 1996; Carrigan et al., 1996; Kalinowski, 2011; Sun and Carrigan, 2014; Bourret et al., 2019). Noble gases produced by nuclear fission are hard to contain and tend to migrate to the surface where they can be detected via atmospheric monitoring, making them key components for compliance monitoring for the comprehensive nuclear-test-ban treaty (CTBT) (Carrigan and Sun, 2014; De Geer, 1996; Jordan et al., 2014, 2015; Perkins and Casey, 1996). In particular, radioxenon is an abundant fission product important to nuclear test detection because the half-lives of its isotopes are generally long enough to be detected at extended distances from a detonation site (Ringbom et al., 2014). Accurate prediction of noble gas subsurface transport is challenging because we lack understanding of key processes that control transport, including the sorption

* Corresponding author. P.O. Box 1663, Los Alamos, NM, 87545, USA.
E-mail address: cwneil@lanl.gov (C.W. Neil).
Current Affiliation: Nicholas School of the Environment, Duke University, Durham, NC 27708, USA.
1 Current Affiliation: Science and Analytics Team, The Freshwater Trust, Portland, OR 97205, USA.

https://doi.org/10.1016/j.jenvrad.2022.106905
Received 21 September 2021; Received in revised form 2 March 2022; Accepted 1 May 2022
Available online 19 May 2022

of noble gases to geological materials and the impacts of variable saturation, making it difficult to discriminate environmentally fractionated nuclear test signatures from background radionuclide sources (Bowyer, 2021; Lowrey et al., 2013b; Sun and Carrigan, 2014).

Following an underground nuclear explosion (UNE), gaseous radioisotopes, including xenon and krypton, are initially produced in known ratios according to the independent yields of nuclear fission (Crouch, 1977; England and Rider, 1994). Decay of pre-cursor radionuclides, such as the production of xenon (131m, 133, and 135) from antimony, tellurium and iodine, can lead to a cumulative yield several orders of magnitude higher than the instantaneous yield. Due to the varying precursor half-lives involved, the time it takes to reach maximum fission yield ranges from 10.7 h, 2.78 days, to 14.4 days for ^{135}Xe, ^{133}Xe and ^{131m}Xe respectively, and signature discrimination utilizes ratios of these xenon isotopes. It is therefore vital that we consider how diffusive transport of both xenon and its precursors following a UNE will impact barometric pumping efficiencies, as well as the potential impact of diffusive transport differences on measured isotopic ratios at different times, which will include varying degrees of ingrowth from parent radionuclide decay. While diffusion is not expected to be the primary transport mechanism for gaseous signatures following a UNE, it plays a critical role in the rate at which barometric pumping occurs thanks to a processes called "ratcheting" (Bourret et al., 2019; Carrigan et al., 2016; Harp et al., 2019; Nilson et al., 1991; Sun and Carrigan, 2016). During this process, gas which is transporting within fractures due to barometric pumping will diffuse into the surrounding rock matrix, which acts as relatively immobile storage during barometric cycles. Thus, accurate quantification of diffusion rates and a thorough understanding of matrix-gas interactions is needed to model gas behavior in the field.

For example, Lowrey et al. (2013a) modeled the impact of mass transport-induced fractionation on gas seepage from a UNE. Their study employs the previously established multi-isotope discrimination method using xenon isotopic activity ratio relationships (Kalinowski et al., 2010). According to this method, a xenon signature was considered indicative of a nuclear test if it fell in an area bounded by the ratio of xenon isotopes expected for a "fully fractioned" nuclear test, where there is no contribution from parent decay, and by the ratio expected for a "non-fractioned" test, where all isotopes which decay to xenon contribute to the measured signal. They found that by incorporating mass transport, xenon isotope ratios fell outside of this range 20% of the time. However, these models did not account for the potential presence of water in the bulk matrix medium, which can further complicate transport due to partitioning between gas and liquid phases (Jordan et al., 2015; Harp et al., 2018; Sleep and Sykes, 1989).

Because US UNEs are buried deeply enough to prevent radiation containment failures, even tests carried out above the water table can still contain a significant percentage of water (Hoffman et al., 1977). Pawloski (1981) determined the total water content of different lithologic units at the Nevada National Security Site (NNSS), where many historic US nuclear tests were conducted, and found that the average total water content of volcanic tuff was 19 ± 4% by mass, compared with 14 ± 5% by mass for alluvium. For these measurements, the confidence internal is the standard deviation. A UNE event itself can also alter local hydrology (Wohletz et al., 1999; Knox et al., 1965). For example, a 1962 UNE at NNSS in unsaturated tuff above the water table increased the groundwater water level by 17 m in a well 307 m away from ground zero and elevated hydraulic heads persisted in this area for more than 15 months (Knox et al., 1965). Although this anomaly was first measured 40 days after the explosion, it is hypothesized to have occurred shortly after the explosion due to dynamic compaction of water-containing pores. Such a large increase in the elevation of groundwater in the vicinity of a UNE detonation site is expected to greatly increase the saturation of surrounding rocks, and can thus alter the transport conditions for fission products.

Bench-scale gas transport experiments have previously been used to examine noble gas transport in the context of post-UNE signature transport (Broome et al., 2016). Additionally, laboratory studies have shown non-trivial Xe sorption on various geologic media including shale, dolomite, limestone, and sand (Byers et al., 2019; Paul, 2017; Paul et al., 2018). One geologic media of particular interest is zeolites. A recent study found that natural zeolites in zeolitic tuff can sorb noble gases, and this sorption is particularly significant for Xe (Feldman et al., 2020). Many historical US tests were conducted in zeolite-rich subsurface strata, common within Pahute Mesa at NNSS, meaning this interaction can be important for understanding and modeling historic gas transport data (Moncure et al., 1981). Both sorption and diffusivity of gases, including Xe and SF_6, have been explored through laboratory investigations for dry and partially-saturated zeolitic tuff (Feldman et al., 2020; Paul et al., 2020). However, diffusivity of partially-saturated zeolitic tuff was measured at nearly fully-saturated conditions (Paul et al., 2020). There is no comprehensive study relating gas transport through zeolitic tuff to the level of rock saturation at multiple intervals between dry and fully saturated. In particular, we expect that the presence of water will impact reported noble gas sorption by zeolites.

Table1
QXRD results for zeolitic non-welded tuff core indicates that the core is mainly zeolites.

QXRD for Zeolitic Tuff	
Feldspar	*Percent*
Plagioclase	2.7
Alkali feldspar	13.5
Zeolite	
Heulandite	30.8
Mordenite	38.9
Analcime	2.1
Silica	
Cristobalite	2.0
Quartz	1.0
Clay	
Montmorillonite	2.7
Amorphous	6.3
SUM	100.0

The goal of the current study is thus to investigate both the impact of sorption by zeolites in zeolitic tuff on gas transport, as well as how pore water impacts both transport and sorption. To achieve this goal, we examine the diffusion of a mixture of gases through a zeolite-rich rock core at varying degrees of saturation using a benchtop laboratory experimental apparatus. Prior to experimentation, the core was characterized using quantitative X-ray diffraction (QXRD) and helium porosimetry. The gas mixture includes stable krypton and xenon noble gases and SF_6, a common tracer gas used in the field at NNSS to measure geologic properties for simulation of noble gas transport (Carrigan et al., 1995). Diffusion measurements are augmented by small-angle neutron scattering (SANS) measurements, allowing us to infer how sorption processes are impacted by variable saturation.

2. Methods

2.1. Rock core sample

Core samples were taken from the UE-20az-NG-4 core hole on Pahute Mesa at the NNSS at a depth of 440.65–440.83 m. A map of the NNSS can be found in Fig. S1 of the SI. The lithologic unit at this depth is zeolitic non-welded tuff from the Calico Hills zeolitic composite unit (Bourret et al., 2020). Porosity along this unit was measured using helium porosimetry and was found to vary between 16.7% and 32.7%, with an average porosity of 21.6%. These data can be found in Table S1 in the Supporting Information (SI). The mineralogy of the core was further examined using quantitative X-ray diffraction (QXRD) (Table 1). The QXRD spectrum can be found in Fig. S2 in the SI. Samples were run on a Siemens D-500 X-ray diffractometer using CuKα radiation (Bruker AXS,

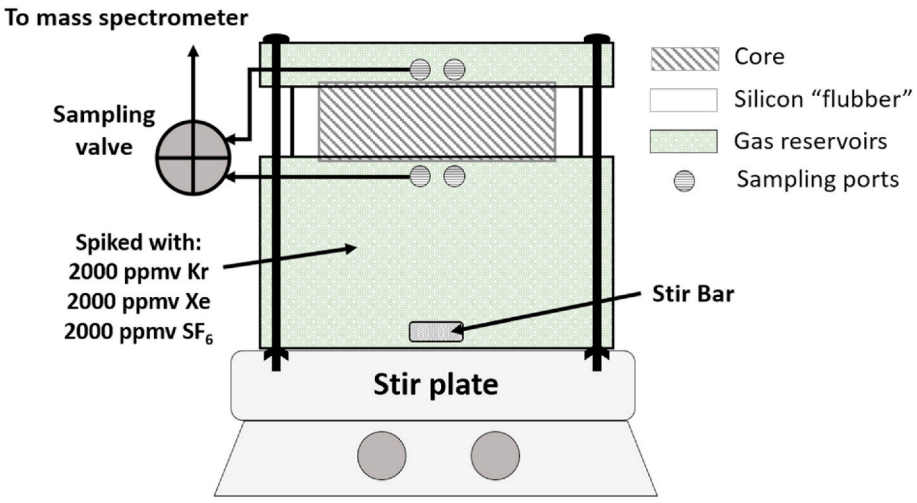

Fig. 1. Diffusion cell schematic.

Madison, WI, USA) with alumina powder (Al_2O_3) as an internal standard. Peak identification was accomplished using JADE software's search-match function (Materials Data, Inc., Livermore, CA, USA). Results indicated that the zeolites present in the rock were primarily mordenite and heulandite, which combined make up nearly 70% of the rock. Both are sodium and calcium aluminosilicate minerals frequently associated with one another in nature and are assumed to be alteration products of once abundant volcanic glass. (Meier, 1961). The main difference between the two is that mordenite has a higher ratio of silicon to aluminum. Other minerals detected using XRD include cristobalite, quartz, plagioclase, alkali feldspar, and montmorillonite.

2.2. Diffusion cell set up

Prior to setting up the diffusion experiments, we cut the rock core into two 5-cm sections and trimmed the circular faces to ensure a uniform, flat surface was in contact with either side of the diffusion cell. The non-face radial edges of the core were coated with a UV-curable polymer (UV15X-6NONMED-2, Master Bond, Inc., Hackensack, NJ, USA) to prevent gas migration along the radial edge of the cylindrical samples. After fully curing in sunlight, the rectangular faces were coated with a silicone primer while the circular top and bottom faces of the core were covered with tape to prevent contact with silicone. The core was placed in a square mold and Room Temperature Vulcanization (RTV) silicone (SILPAK, Inc. Pomona, CA, USA) was added. The core sections were left overnight to allow the silicone to cure and form a molding around the core.

The molded silicone acts as a gasket to seal off the two halves of the diffusion cell, which consists of two cylindrical reservoirs machined out of plexiglass (Fig. 1). The smaller reservoir has a volume of 75 mL and the larger has a volume of 500 mL. Both reservoirs have two sampling ports and an O-ring to help fully seal the chamber against the silicone around the core. The core is placed between the two reservoirs and secured tightly with screws. We tested the potential for preferential Xe sorption to plexiglass and silicone by measuring the concentration loss for the three gases in a sealed diffusion chamber, and found that there was no preferential sorption (Fig. S3 in the SI).

Gas concentrations are measured using a Pfeiffer Vacuum OmniStar GSD 320 mass spectrometer (Pfeiffer Vacuum, Aßlar, Germany). The mass spectrometer (MS) is attached to one of the sampling ports of both reservoirs through a Valco dead-end selector valve and a needle is placed in the other port to prevent the formation of a vacuum while the MS samples at a rate of approximately 0.40 mL/min. To minimize the volume of gas sampled, the selector valve was programmed to allow intermittent sampling of the diffusion cell. While sampling over the 20 h period dilutes the gas concentration, modeling will account for this dilution. In addition, regular monitoring of concentration in both the spiked and sampled chambers gives an accurate view of the changing driving forces for diffusion with time as the system is sampled.

The first experiment is run with a completely dry core. To begin the experiment, we spike the large reservoir, which contains ambient air, with 1 mL each of stable xenon (Xe), krypton (Kr), and SF_6 tracers while measuring their ion current, which correlates with their masses on the spectrometer. This injected volume corresponds with a concentration of 2000 parts per millions by volume (ppmv) for the three gases. Although there may be some variation in concentration due to slight differences in the injected gas amounts, we do not expect these differences to substantially impact the relative transport of the gases. Once the ion current (i.e., concentration) reaches a constant value (within several minutes), we record the concentration as the initial concentration, C_0 (i.e., $C_0(t = 0)$). Next, we automated the process of moving a selector valve to switch between measuring the spiked and smaller reservoir, such that the small reservoir is measured for 1 min every 10 min to monitor breakthrough and the spiked reservoir is measured for 2 min every hour to monitor changes in the C_0 concentration (i.e., $C_0(t)$). We found that running the experiments for 20 h allows the breakthrough curve to level off. A magnetic stirrer continually mixes the spiked cell (Fig. 1) to maintain a homogenous gas mixture and prevent gravity separation of the gases.

The saturations used in the study are 0 (core which is dried in oven until mass stops changing), 17, 40, 85, and 100% (fully) saturated. Partial saturations of 17–85% were calculated as percentages of the total water required for 100% saturation. To achieve as close to uniform saturation as possible, different saturation methods were employed. To achieve 17% saturation, air saturated with water vapor is pulled through the core using a vacuum. The vacuum side is regularly switched and the core is weighed to monitor uptake until it reaches 17% saturation. For higher degrees of saturation (40%, 85% saturated), the core is put under vacuum then submerged in water until the target water mass is gained within the core (Veland, 2017). The core is then allowed to sit for 4 weeks while rotating regularly to more evenly distribute water in the pore spaces. For the fully saturated rock, the core is submerged in water and placed under vacuum, and saturation is monitored by measuring the core weight until it stops increasing (Telfeyan et al., 2018). For all experiments, Los Alamos County tap water is used to minimize rock dissolution, as it contains dissolved silica, bicarbonate and other salts (Neil et al., 2020a). The composition of the tap water and the masses of the rock cores at different saturations can be found in Tables S2 and S3 in the SI.

Between runs, the cores are placed in a vacuum oven until their mass stops changing, at which point they are assumed to be dry. While in the

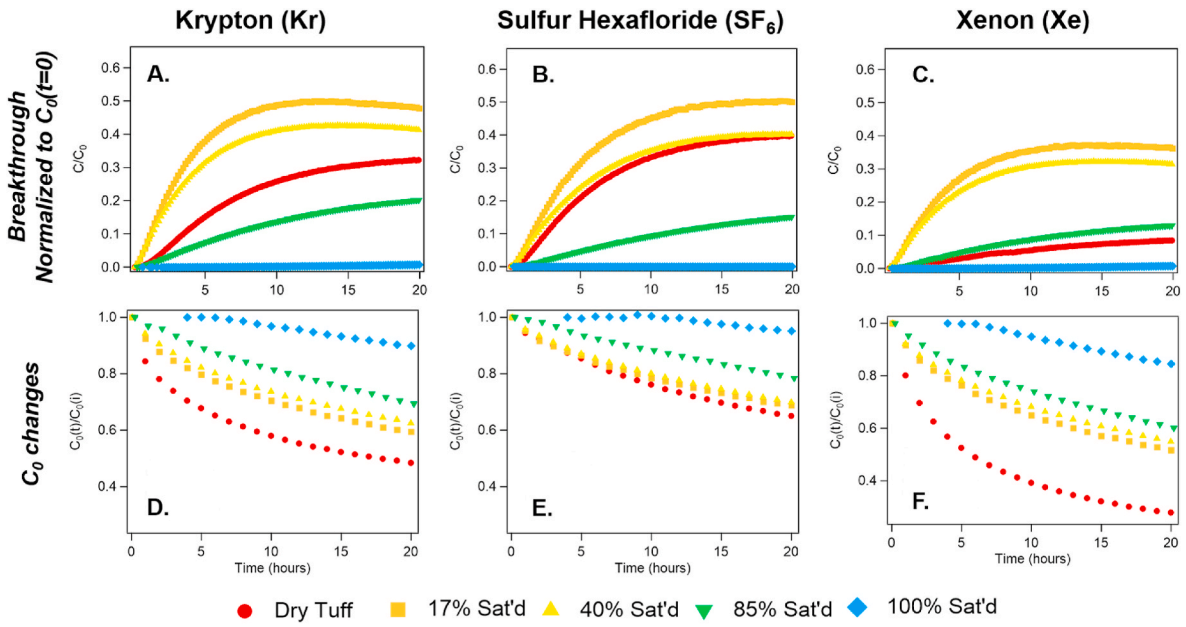

Fig. 2. Diffusion breakthrough curves for (A) Kr, (B) SF_6, and (C) Xe, normalized to the initial measured C_0 ($C_0(t = 0)$); Changes in the spiked concentration with time for (D) Kr, (E) SF_6, and (F) Xe.

vacuum oven, the temperature is maintained below 40 °C to prevent mineral phase transformation (Feldman et al., 2020), therefore some residual or tightly-bound water could still exist. Pawloski (1981) found that free water accounted for 60–90% of the total water content in tuff samples taken from the NNSS, while tightly bound water accounted for 2–33%. Although some water may remain in the rock core sample, this quantity is assumed to be constant between runs, as the drying method was consistent, and masses of the dried samples did not vary significantly. Replicate measurements of dry diffusion were carried out for the two core sections to confirm reproducibility and ensure the sections behaved similarly. These breakthrough graphs can be found in Fig. S4 in the SI. Replicate measurements showed nearly identical trends in gas breakthrough, however the C/C_0 at 20 h varied slightly between runs from 0.3 to 0.4 for SF_6, 0.25–0.35 for Kr and 0.05–0.1 for Xe. Possible sources for this variation include instrumentation error, as well as small changes in environmental conditions such as temperature and atmospheric pressure, which can occur in the laboratory. However, we are confident that the changes observed with varying saturation exceed this error because (1) changes are mostly larger than the 0.5–0.1 variance observed between dry replicates; (2) changes to the shape of the breakthrough curve occur, which was not seen between replicates; and (3) gas breakthrough trends relative to each other change dramatically with saturation, where trends were nearly identical between replicates.

2.3. Nanoporosity measurement with small-angle neutron scattering (SANS)

When porous media becomes saturated with water, not all pores will be filled to the same extent due to differences in pore size, connectivity and/or their chemical nature. To investigate this effect for the zeolitic non-welded tuff used in our transport experiments, we conduct small-angle neutron scattering (SANS) experiments on the NG7 30-m SANS instrument (Glinka et al., 1998) at the NIST (National Institute of Standards and Technology) Center for Neutron Research (NCNR).

During SANS, a beam of neutrons is passed through a sample of interest, where it is elastically scattered by interactions with nuclei in the sample. Neutron scattering and spectroscopic techniques, including SANS, are sensitive to the isotopic composition of the sample (Xu et al. 2020). The scattering length varies with isotope, and the scattering length density (SLD) of a material can thus be calculated from the sum of scattering lengths of atoms in a given volume using its isotopic and elemental composition and density. SLD can vary drastically between isotopes of the same element. For example, the SLD of D_2O is 5.8×10^{-10} cm^{-2}, while the SLD of H_2O is -0.56×10^{-10} cm^{-2}. The positive sign for deuterium implies a repulsive interaction potential resulting in a spherical scattering wave that is out of phase with the incident beam plane wave function, whereas the negative sign for hydrogen implies an attractive potential and a scattering in phase (Shull et al., 1948).

Scattering differences between hydrogen and deuterium allow the technique of contrast matching to be applied. According to this technique, a mixture of D_2O and H_2O can be used as the pore filling fluid, with their ratios adjusted such that the average SLD is equal to that of the rock matrix. We first determine the SLD, ρ, of the matrix by measuring the SANS spectra for the tuff powder saturated with various D_2O/H_2O ratios. The spectra are compared and the one with the lowest intensity is considered to match the contrast of the rock matrix. For our sample, this ratio is 70/30 D_2O/H_2O (SLD $= 4.31 \times 10^{-10}$ cm^{-2}). The use of powder rather than intact core for SANS experiments is not expected to significantly impact the underlying pore size distribution (Kuila and Prasad, 2013). However, the increased exposed mineral surface area of power versus intact rock can lead to more extensive interactions with water (Al Hinai et al., 2014), as more pores will be exposed to the water than what may be accessible through the pore network of the intact rock. While such an effect may lead to more extensive interactions, we expect observed differences in pore accessibility to hold for intact rock samples where nanopores are exposed to water.

Scattering intensity is proportional to the average contrast squared, $\overline{\Delta\rho^2}$, over the volume sampled by the neutron beam. Here, $\Delta\rho = \rho_p - \rho_m$, where the subscript p refers to the SLD of the pore and m refers to the SLD of the surrounding matrix. The SLD of an empty pore is approximately 0, meaning that scattering is maximized when pores are empty, i.e., $\Delta\rho$ is at its highest value. When the contrast matching fluid is introduced, the scattering intensity from accessible pores becomes negligible. Scattering from pores inaccessible to the fluid is not affected. Thus, the method provides a means to discriminate between accessible and inaccessible pores. More information on SANS theory can be found in previous publications (Neil et al., 2020b; 2020c).

We measured the SANS spectra for zeolitic tuff powder that is dry,

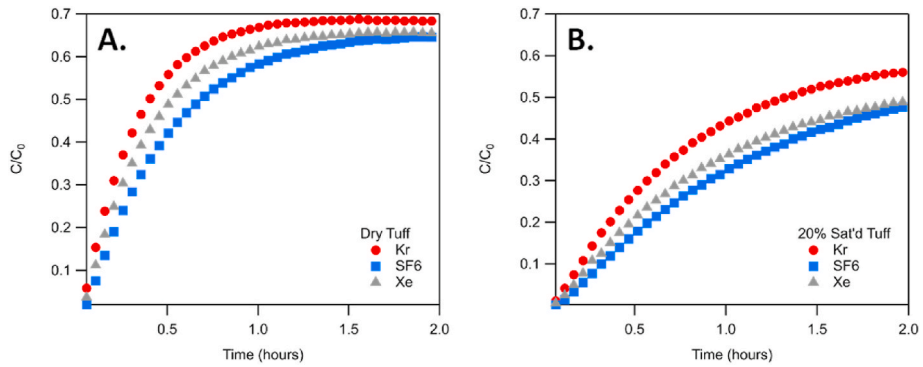

Fig. 3. Diffusion of Kr, SF_6, and Xe were measured through a tuff core which did not contain zeolites under (A) dry and (B) 20% saturated conditions.

and rock powder with 10 μL or 20 μL of contrast matching water added. The partial saturations are calculated by measuring water uptake, to be 46% for 10 μL and 93% for 20 μL. We use NCNR's data reduction package to reduce the raw SANS data to differential cross section per radian per unit volume (cm^{-1}) as a function of momentum transfer, Q ($Å^{-1}$), known as the scattering function (Kline, 2006). Q is defined as:

$$Q = 4\pi \frac{sin\theta}{\lambda(Å)} \quad (1)$$

Here, λ (Å) is the incident neutron beam wavelength and 2θ is the scattering angle. Structural information such as pore size and internal surface roughness were determined by model fitting the scattering functions (Ilavsky and Jemian, 2008). Comparison between these distributions indicates which pore sizes are being filled as saturation increases.

3. Results and discussion

3.1. Zeolites impact gas breakthrough trends

Trends in the breakthrough and fractionation of gaseous species through the rock core give preliminary insight into the impact of saturation on transport. In Fig. 2A–C, we present experimental breakthroughs for Kr, SF_6, and Xe at different saturations, normalized to the initial measured C_0 value, $C_0(t = 0)$. Fig. S5 in the SI contains graphs showing breakthrough differences for the three gases within each saturation system. Under dry conditions, SF_6 has the fastest breakthrough, while Kr is slightly slower and Xe is the slowest. Increasing saturation from dry to 17% unexpectedly results in faster breakthrough for all three gases. This trend in breakthrough behavior is not observed in the absence of zeolites (Fig. 3). However, when saturation is increased further to 40%, breakthrough for the three gases drops relative to the 17% saturation system, but remains faster than in the dry system. Once saturation is increased again to 85%, breakthrough for Kr and SF_6 is slower than that in the dry system, but for Xe, breakthrough at 85% saturation remains faster than in the dry system. 85% is also the saturation point where Xe and SF_6 begin to transport similarly. Finally, for the fully saturated system, breakthrough is slowest for all three gases, with slightly faster breakthrough of Xe and Kr relative to SF_6 (Fig. S5F in the SI).

To analyze these experiments, we first explore whether these trends can result from differences in water partitioning. Xe has the highest Henry's Law constant (liquid concentration (mol of tracer/kg of water) divided by gas concentrations (in partial pressure, bar^{-1})) at 0.0043 mol $kg^{-1}{\cdot}bar^{-1}$, compared to 0.0025 mol $kg^{-1}{\cdot}bar^{-1}$ for Kr and 0.00024 mol $kg^{-1}{\cdot}bar^{-1}$ for SF_6 (Sander, 2000). Thus, we might expect that under higher partial saturations, Xe would break through more slowly due to increased interactions with water. However, we find that this is not the case, as Xe breakthrough in the dry system is slower than that in the 17%, 40%, and 85% saturated systems. On the other hand, for the fully saturated system, higher Henry's law constants promote transport, which is expected to occur primarily in the water phase. The relatively faster breakthroughs of Kr and Xe compared to SF_6 in the fully saturated system make this apparent.

Although our study only considered diffusive transport through intact rock, a small scale field experiment by Stroujkova et al. (2020) also showed faster transport of Xe than SF_6 in the absence of advective transport from a cavity below the water table. Stroujkova et al. (2020) suggest that due to the higher Henry's Law constant of Xe, transport within the aqueous phase may allow Xe to transport faster than SF_6. Direct comparison between our results and this study are hard because of the absence of barometric pumping effects and induced fracture flow. However, diffusion is one piece of the puzzle which can be incorporated to explain some of the observed trends in more complex natural systems.

3.2. Water uptake reduces sorption by tuff rocks

Since water partitioning cannot explain the different breakthrough

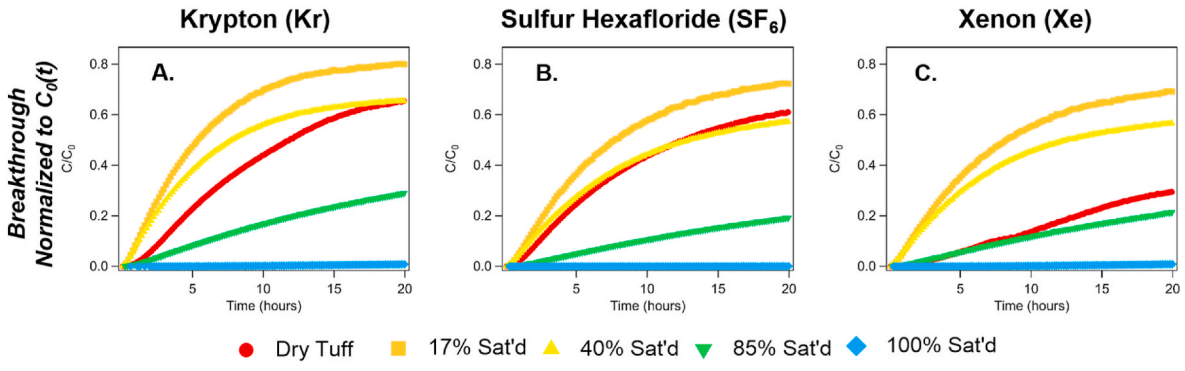

Fig. 4. Diffusion breakthrough curves for (A) Kr, (B) SF_6, and (C) Xe, normalized to the measured C_0 at each time point, $C_0(t)$.

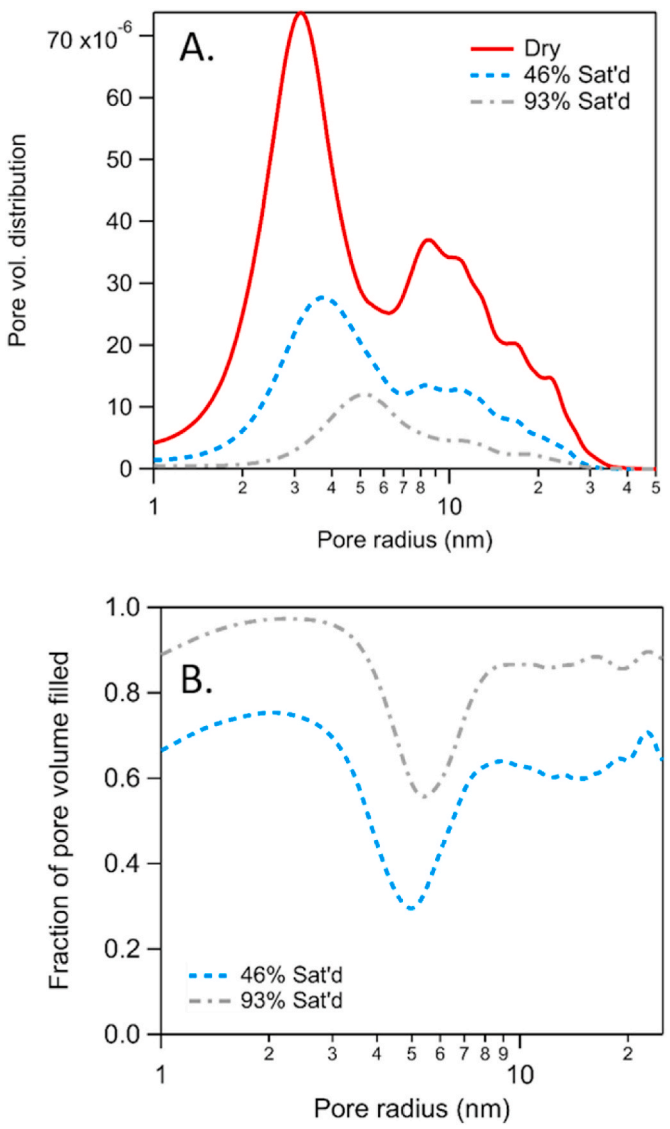

Fig. 5. (A) Fitted pore size distribution for zeolitic tuff with increasing water content, showing that smaller pores will preferentially fill first. Fitting used Irena's maximum entropy method. Comparison between fitting methods can be found in the SI. (B) Fraction of filled pores across the fitted size range. Size is cut off at 25 nm because ratios become skewed as the distribution approaches zero.

trends, we instead explored whether these differences could be related to interactions between natural zeolites and gases, as observed previously for zeolitic tuff (Feldman et al., 2020). Fig. 2D–F presents the changes in the spiked concentration in the large diffusion chamber, monitored through hourly measurements and presented as the ratio of $C_0(t)$ to $C_0(t = 0)$. These graphs clearly demonstrate interactions between the zeolitic tuff core and gases. Of note, for the dry xenon system, the C_0 concentration drops to nearly 30% of the initial spiked value after the 20-h transport period. This drop is larger than that of Kr (47% remaining) and SF_6 (64% remaining), indicating preferential sorption of Xe, in line with previous observations (Feldman et al., 2020). Upon partial saturation to 17%, there is a dramatic decrease in Xe uptake by the core, although there is still a larger C_0 decrease for Xe (52% remaining) relative to Kr (59% remaining) and SF_6 (69% remaining). This trend continues, with increasing saturation leading to a smaller drop in C_0 for all three gases, although this drop is always most significant for Xe. Thus, trends such as the faster breakthrough for gases in the 17% saturated system are likely related to the stronger concentration gradient in that system, as a result of decreased sorption.

To further understand how uptake by zeolitic tuff alters the driving force for diffusion, we normalize the diffusion curves to the changing reservoir chamber concentration, $C_0(t)$, rather than $C_0(t = 0)$, by fitting the concentration curves using a polynomial function (Fig. 4). Interestingly, the diffusion curves for SF_6 and Xe are nearly identical for all saturated systems when normalized in this manner, while for the dry system, breakthrough remains significantly lower for Xe. This is in line with the similar masses and reported diffusivities of Xe and SF_6 (Byers et al., 2018). The faster diffusion of Kr (Fig. 4A) is also consistent with the reported higher diffusion coefficient for Kr ($10^{-0.770}$ cm^2/s) in nitrogen compared with Xe and SF_6 ($10^{-0.855}$ cm^2/s and $10^{-0.9393}$ cm^2/s, respectively) and is in line with differences in their molecular size, as the kinetic diameter of Kr is less than that of Xe and SF_6 (Breck, 1973; Marrero and Mason, 1972).

3.3. *Zeolite pores fill preferentially upon water exposure*

Although adjusting for changes in C_0 leads to more logical breakthrough trends under partial to fully saturated conditions, for all three gases, the dry breakthrough is still significantly slower. This observation indicates that initial partial saturation up to at least 17% greatly decreases interactions between zeolitic tuff and gases, as observed in C_0 changes (Fig. 2D–F). SANS results give some insight into this observed phenomenon. Fitted pore size distributions (Fig. 5A) show that when water with SLD matching that of the tuff matrix is introduced to a zeolitic tuff powder sample, a significant portion of the smallest pores are filled, as indicated by the decrease in their abundance relative to larger pores. Fig. 5B shows the fraction of pores that are filled. While logically it may seem easier to fill larger sized pores, results show that at both saturations, greater than 10% more of the smaller pores are filled.

These pores have a radius of approximately 3 nm, consistent with the previously reported peak pore size of naturally-occurring zeolites, between 2 and 4 nm in radius (Milićević, et al., 2013). While zeolite framework channel diameters are typically 3–8 Å, and thus below the SANS detection limit, these pores fall into the mesoporous range, reported for zeolites to be characteristic of slot pores formed due to the existence of zeolite cleavage planes (Mansouri et al., 2013). This finding suggests that small pores, possibly belonging to natural zeolites, preferentially fill upon partial saturation with water, supporting the dramatic change in gas transport behavior upon partial saturation to 17%. This behavior is also supported by a reported water retention curve for zeolite, which indicates that water saturations below 20% require a suction pressure such that this water is unavailable to plants (Szatanik-Kloc et al., 2021). Reduced SANS scattering spectra (Fig. S6) and a comparison between Irena size distribution fitting using maximum entropy (Fig. 5) and total non-negative least squares (Fig. S7B) can be found in the SI. Both methods show that upon partial saturation, the most significant drop in pore abundance occurs for the 3 nm radius pores. More information on the SANS fitting procedure can be found in our previous publications (Neil et al., 2020b; 2020c).

This observation provides critical new insight into how the presence of zeolites and water can impact the transport of nuclear signature gases in the field. In particular, increased retardation of Xe during subsurface transport due to sorption by zeolites at low water saturations will lead to signature fractionation, altering the elemental ratios expected from a subsurface test. To determine how large of an effect the sorption mechanism will have on field scale transport, we are now incorporating these new findings into models which also include pressure-driven advective transport away from the cavity and barometric pumping to pull gases to the surface. Understanding this process and properly incorporating it into subsurface transport models is crucial to accurately constraining the expected elemental ratios utilized to discern a nuclear test from other radioisotope sources. In addition, these results show the importance of experimentally investigating specific interactions between the rock matrix and gases of interest and characterizing how these interactions may be different from chemical tracers used in the field.

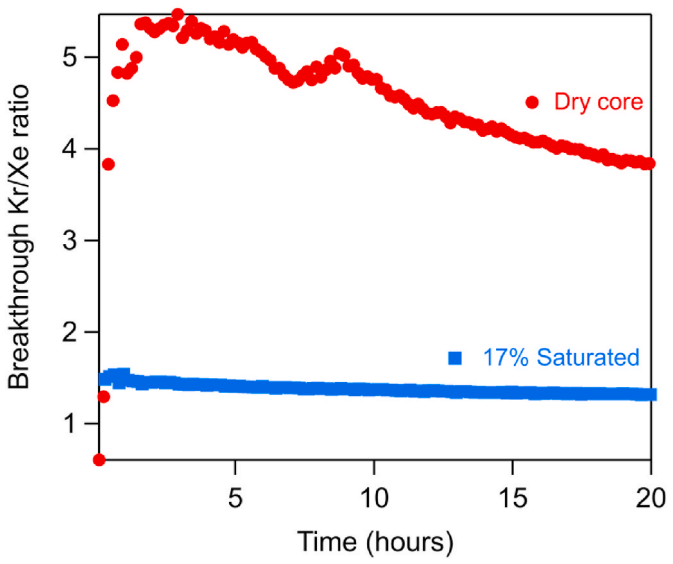

Fig. 6. Ratio of Kr/Xe breaking through core over the 20 h diffusion study. A much higher ratio is present in the dry core due to low Xe diffusion and more significant Xe sorption.

4. Conclusions

Transport models that are accurate enough for use as diagnostic tools to interpret nuclear signatures must include the physical processes and geochemical reactions controlling transport in subsurface environments. We show that transport of Xe, a key nuclear event signature, will be significantly impacted by sorption to zeolites, and that the extent of sorption greatly depends on the saturation state of the media. More significant sorption of Xe during transport can explain observed trends in field measurements of SF_6 and Xe transport. In 2013 and 2016, large scale transport experiments were conducted at the NNSS wherein Xe and SF_6 were injected into a UNE chimney in the U20az testbed (Johnson et al., 2019; Olsen et al., 2016). Both migration studies found that following subsurface transport, SF_6 was enriched relative to Xe. As zeolitic tuff is present in this testbed (Heath et al., 2021), sorption interactions observed in this study may contribute to SF_6 enrichment.

As a result of this sorption interaction, transport of Xe in dry zeolite-rich formations will be significantly slower than that of Kr (Fig. 6), leading to fractionation between Xe and Kr. Additionally, fractionation can occur between Xe isotopes due to the different half-lives of these isotopes, altering the isotopic ratios used to discriminate between UNEs and background sources. Through neutron scattering, we observe that a small amount of water greatly reduces sorption, enhacing transport due to the preferential uptake of water by small pores, likely natural zeolites, upon saturation. These results indicate the important role of saturation in predicting both the overall transport and fractionation of signatures, and highlights the urgent need to accurately measure *in situ* saturation in the subsurface during future field scale transport experiments. As volcanic tuff at the NNSS contains 19 ± 4% water by mass on average (Pawloski 1981), Xe will likely not adsorb to the extent observed for dry zeolite tuff. However, sorption effects were still observed at partial saturations. Additionally, it is important to consider how saturation will vary with depth, and how it may change as a result of the UNE itself.

The collected data are being used to improve current models by quantifying both sorption and effective diffusion coefficients of these signature gases through zeolitic tuff. As historical tests have taken place in similar strata, our improved understanding of signature gas transport for these scenarios will allow us to make inferences which can be applied in support of nonproliferation science. Furthermore, this study can be expanded to examine interactions of gases with different rock types and explore fractionation and potential sorption differences between different gas species and isotopes, supplying critically-needed data on nuclear signature gas transport.

Declaration of competing interest

The authors declare that they have no known competing financial interests or personal relationships that could have appeared to influence the work reported in this paper.

Acknowledgements

This research was funded by the National Nuclear Security Administration, Defense Nuclear Nonproliferation Research and Development (NNSA DNN R&D) and the Defense Threat Reduction Agency (DTRA). The authors acknowledge important interdisciplinary collaboration with scientists and engineers from LANL, LLNL, MSTS, PNNL, and SNL. The authors also thank the Underground Nuclear Explosion Signatures Experiment team, a multi-institutional and interdisciplinary group of scientists and engineers, for providing the zeolitic tuff core and core characterization. The authors acknowledge the Center for Neutron Research (CNR) at National Institute of Standards and Technology for access to Small Angle Neutron Scattering (SANS). Los Alamos National Laboratory, an affirmative action/equal opportunity employer, is operated by Triad National Security, LLC, for the National Nuclear Security Administration of U.S. Department of Energy (Contract No. 89233218CNA000001). By approving this article, the publisher recognizes that the U.S. Government retains nonexclusive, royalty-free license to publish or reproduce the published form of this contribution, or to allow others to do so, for U.S. Government purposes. Los Alamos National Laboratory requests that the publisher identify this article as work performed under the auspices of the U.S. Department of Energy. Los Alamos National Laboratory strongly supports academic freedom and a researcher's right to publish; as an institution, however, the Laboratory does not endorse the viewpoint of a publication or guarantee its technical correctness. The identification of any commercial product or trade name does not imply endorsement or recommendation by the National Institute of Standards and Technology. The authors would like to thank the reviewers, particularly Charles Carrigan, for their thoughtful reviews of our manuscript.

Appendix A. Supplementary data

Supplementary data to this article can be found online at https://doi.org/10.1016/j.jenvrad.2022.106905.

References

Al Hinai, A., Rezaee, R., Esteban, L., Labani, M., 2014. Comparisons of pore size distribution: a case from the Western Australian gas shale formations. J. Unconvent. Oil Gas Resour. 8, 1–13.

Auer, L.H., Rosenberg, N.D., Birdsell, K.H., Whitney, E.M., 1996. The effects of barometric pumping on contaminant transport. J. Contam. Hydrol. 24 (2), 145–166.

Bourret, S.M., Kwicklis, E.M., Miller, T.A., Stauffer, P.H., 2019. Evaluating the importance of barometric pumping for subsurface gas transport near an underground nuclear test site. Vadose Zone J. 18 (1).

Bourret, S.M., Kwicklis, E.M., Harp, D.R., Ortiz, J.P., Stauffer, P.H., 2020. Beyond Barnwell: applying lessons learned from the Barnwell site to other historic underground nuclear tests at Pahute Mesa to understand radioactive gas-seepage observations. J. Environ. Radioact. 222, 106297.

Bowyer, T.W., 2021. A review of global radioxenon background research and issues. Pure Appl. Geophys. 178 (7), 2665–2675.

Broome, S.T., Cashion, A.T., Feldman, J.D., Sussman, A.J., Swanson, E.M., Wilson, J., Heath, J.E., Kuhlman, K.L., 2016. *Laboratory Noble Gas Migration Experiments Through Rock* (No. SAND2016-12586C). Sandia National Lab.(SNL-NM), Albuquerque, NM (United States).

Breck, D.W., 1973. Zeolite Molecular Sieves: Structure, Chemistry, and Use. John Wiley & Sons.

Byers, M.F., Paul, M.J., Haas, D.A., Biegalski, S.R., De Luna, B.A., Barth, B.S., 2018. Evaluation of carbon tetrafluoride as a xenon surrogate for underground gas transport. J. Radioanal. Nucl. Chem. 318 (1), 465–470.

Byers, M.F., Haas, D.A., Barth, B.S., Lowrey, J., 2019. Adsorption of tracer gases in geological media: experimental benchmarking. J. Radioanal. Nucl. Chem. 322 (3), 1621–1626.
Carrigan, C., Heinle, R., Zucca, J.J., 1995. *The NPE Gas Tracer Test and the Development of On-Site Inspection Techniques* (No. UCRL-ID-120931; INIS-XA-N—327). Lawrence Livermore National Lab., CA (United States).
Carrigan, C.R., Heinle, R.A., Hudson, G.B., Nitao, J.J., Zucca, J.J., 1996. Trace gas emissions on geological faults as indicators of underground nuclear testing. Nature 382 (6591), 528.
Carrigan, C.R., Sun, Y., 2014. Detection of noble gas radionuclides from an underground nuclear explosion during a CTBT on-site inspection. Pure Appl. Geophys. 171 (3–5), 717–734.
Carrigan, C.R., Sun, Y., Hunter, S.L., Ruddle, D.G., Wagoner, J.L., Myers, K.B., Emer, D. F., Drellack, S.L., Chipman, V.D., 2016. Delayed signatures of underground nuclear explosions. Sci. Rep. 6 (1), 1–9.
Crouch, E.A.C., 1977. Fission-product yields from neutron-induced fission. Atomic Data Nucl. Data Tables 19 (5), 417–532.
De Geer, L.E., 1996. Atmospheric radionuclide monitoring: a Swedish perspective. In: Monitoring a Comprehensive Test Ban Treaty. Springer, Dordrecht, pp. 157–177.
England, T.R., Rider, B.F., 1994. ENDF-349 *Evaluation and Compilation of Fission Product Yields 1993*. Los Alamos National Laboratory, LA-UR, pp. 94–3106.
Feldman, J., Paul, M., Xu, G., Rademacher, D.X., Wilson, J., Nenoff, T.M., 2020. Effects of natural zeolites on field-scale geologic noble gas transport. J. Environ. Radioact. 220, 106279.
Glinka, C.J., Barker, J.G., Hammouda, B., Krueger, S., Moyer, J.J., Orts, W.J., 1998. The 30 m small-angle neutron scattering instruments at the National Institute of Standards and Technology. J. Appl. Crystallogr. 31 (3), 430–445.
Harp, D.R., Ortiz, J.P., Pandey, S., Karra, S., Anderson, D., Bradley, C., Viswanathan, H., Stauffer, P.H., 2018. Immobile pore-water storage enhancement and retardation of gas transport in fractured rock. Transport Porous Media 124 (2), 369–394.
Harp, D.R., Ortiz, J.P., Stauffer, P.H., 2019. Identification of dominant gas transport frequencies during barometric pumping of fractured rock. Sci. Rep. 9 (1), 1–9.
Heath, J.E., Kuhlman, K.L., Broome, S.T., Wilson, J.E., Malama, B., 2021. Heterogeneous Multiphase Flow Properties of Volcanic Rocks and Implications for Noble Gas Transport from Underground Nuclear Explosions. Vadose Zone Journal, e20123.
Hoffman, D.C., Stone, R., Dudley Jr., W.W., 1977. *Radioactivity in the Underground Environment of the Cambric Nuclear Explosion at the Nevada Test Site* (No. LA-6877-MS). Los Alamos National Laboratory, NM (United States).
Ilavsky, J., Jemian, P.R., 2008. Irena and Indra SAXS data analysis macros, including maximum entropy. http://www.uni.aps.anl.gov/~ilavsky/irena.html.
Johnson, C., Aalseth, C.E., Alexander, T.R., Bowyer, T.W., Chipman, V., Day, A.R., Drellack, S., Fast, J.E., Fritz, B.G., Hayes, J.C., Huckins-Gang, H.E., 2019. Migration of noble gas tracers at the site of an underground nuclear explosion at the Nevada National Security Site. J. Environ. Radioact. 208, 106047.
Jordan, A.B., Stauffer, P.H., Zyvoloski, G.A., Person, M.A., MacCarthy, J.K., Anderson, D. N., 2014. Uncertainty in prediction of radionuclide gas migration from underground nuclear explosions. Vadose Zone J. 13 (10).
Jordan, A.B., Stauffer, P.H., Knight, E.E., Rougier, E., Anderson, D.N., 2015. Radionuclide gas transport through nuclear explosion-generated fracture networks. Sci. Rep. 5, 18383.
Kalinowski, M.B., Axelsson, A., Bean, M., Blanchard, X., Bowyer, T.W., Brachet, G., Hebel, S., McIntyre, J.I., Peters, J., Pistner, C., Raith, M., 2010. Discrimination of nuclear explosions against civilian sources based on atmospheric xenon isotopic activity ratios. Pure Appl. Geophys. 167 (4), 517–539.
Kalinowski, M.B., 2011. Characterisation of prompt and delayed atmospheric radioactivity releases from underground nuclear tests at Nevada as a function of release time. J. Environ. Radioact. 102 (9), 824–836.
Kline, S.R., 2006. Reduction and analysis of SANS and USANS data using IGOR Pro. J. Appl. Crystallogr. 39 (6), 895–900.
Knox, J.B., Rawson, D.E., Korver, J.A., 1965. Analysis of a groundwater anomaly created by an underground nuclear explosion. J. Geophys. Res. 70 (4), 823–835.
Kuila, U., Prasad, M., 2013. Application of nitrogen gas-adsorption technique for characterization of pore structure of mudrocks. Lead. Edge 32 (12), 1478–1485.
Lowrey, J.D., Biegalski, S.R., Osborne, A.G., Deinert, M.R., 2013a. Subsurface mass transport affects the radioxenon signatures that are used to identify clandestine nuclear tests. Geophys. Res. Lett. 40 (1), 111–115.
Lowrey, J.D., Biegalski, S.R., Deinert, M.R., 2013b. UTEX modeling of radioxenon isotopic fractionation resulting from subsurface transport. J. Radioanal. Nucl. Chem. 296 (1), 129–134.
Marrero, T.R., Mason, E.A., 1972. Gaseous diffusion coefficients. J. Phys. Chem. Ref. Data 1 (1), 3–118.
Mansouri, N., Rikhtegar, N., Panahi, H.A., Atabi, F., Shahraki, B.K., 2013. Porosity, characterization and structural properties of natural zeolite-clinoptilolite-as a sorbent. Environ. Protect. Eng. 39 (1).
Meier, W.M., 1961. The crystal structure of mordenite (ptilolite). Z. für Kristallogr. - Cryst. Mater. 115 (1–6), 439–450.
Neil, C.W., Telfeyan, K., Sauer, K.B., Ware, S.D., Reimus, P., Boukhalfa, H., Roback, R., Brug, W.P., 2020a. Iodine effective diffusion coefficients through volcanic rock: influence of iodine speciation and rock geochemistry. J. Contam. Hydrol. 235, 103714.
Neil, C.W., Hjelm, R.P., Hawley, M.E., Watkins, E.B., Cockreham, C., Wu, D., Mao, Y., Fischer, T.B., Stokes, M.R., Xu, H., 2020b. Small-angle neutron scattering (SANS) characterization of clay-and carbonate-rich shale at elevated pressures. Energy Fuel. 34 (7), 8178–8185.
Neil, C.W., Mehana, M., Hjelm, R.P., Hawley, M.E., Watkins, E.B., Mao, Y., Viswanathan, H., Kang, Q., Xu, H., 2020c. Reduced methane recovery at high pressure due to methane trapping in shale nanopores. Commun. Earth Environ. 1 (1), 1–10.
Nilson, R.H., Peterson, E.W., Lie, K.H., Burkhard, N.R., Hearst, J.R., 1991. Barometric pumping of contaminated gases through fractured permeable media. In: High Level Radioactive Waste Management: Proceedings of the Second Annual International Conference. Proceedings, vol. 1.
Olsen, K.B., Kirkham, R.R., Woods, V.T., Haas, D.H., Hayes, J.C., Bowyer, T.W., Mendoza, D.P., Lowrey, J.D., Lukins, C.D., Suarez, R.D., Humble, P.H., 2016. Noble gas migration experiment to support the detection of underground nuclear explosions. J. Radioanal. Nucl. Chem. 307 (3), 2603–2610.
Paul, M.J., 2017. *Transport and Sorption of Noble Gases in Porous Geological Media* (Doctoral Dissertation).
Paul, M.J., Biegalski, S.R., Haas, D.A., Jiang, H., Daigle, H., Lowrey, J.D., 2018. Xenon adsorption on geological media and implications for radionuclide signatures. J. Environ. Radioact. 187, 65–72.
Paul, M.J., Broome, S., Kuhlman, K.L., Feldman, J., Heath, J., 2020. An experimental method to measure gaseous diffusivity in tight and partially saturated porous media via continuously monitored mass spectrometry. Transport Porous Media 133 (1), 1–22.
Pawloski, G.A., 1981. *Water Contents of Samples from the Nevada Test Site: Total, Free (Natural State to 105°C), and More Tightly Bonded (105 to 700°C)* (No. UCRL-53130). Lawrence Livermore National Lab., CA (USA).
Perkins, R.W., Casey, L.A., 1996. Radioxenons: Their Role in Monitoring a Comprehensive Test Ban Treaty. Pacific Northwest National Lab., Richland, WA (United States). No. DOE/RL-96-51; PNNL-SA-27750).
Ringbom, A., Axelsson, A., Aldener, M., Auer, M., Bowyer, T.W., Fritioff, T., Hoffman, I., Khrustalev, K., Nikkinen, M., Popov, V., Popov, Y., 2014. Radioxenon detections in the CTBT international monitoring system likely related to the announced nuclear test in North Korea on February 12, 2013. J. Environ. Radioact. 128, 47–63.
Sander, R., 2000. Henry's law constants. In: Linstrom, P.J., Mallard, W.G. (Eds.), NIST Chemistry WebBook, NIST Standard Reference Database Number 69. National Institute of Standards and Technology, Gaithersburg MD, p. 20899.
Shull, C.G., Wollan, E.O., Morton, G.A., Davidson, W.L., 1948. Neutron diffraction studies of NaH and NaD. Phys. Rev. 73 (8), 842.
Sun, Y., Carrigan, C.R., 2016. Thermally driven advection for radioxenon transport from an underground nuclear explosion. Geophys. Res. Lett. 43 (9), 4418–4425.
Sleep, B.E., Sykes, J.F., 1989. Modeling the transport of volatile organics in variably saturated media. Water Resour. Res. 25 (1), 81–92.
Stroujkova, A., Gorman, E., Avendano, S.T., Horne, M., Person, M.A., Hubbard, P., Salerno, J., Carrigan, C.R., Harp, D.R., Stauffer, P.H., 2020. Using SF6 and Xe to monitor gas migration through explosion-generated fracture networks. J. Geophys. Res. Solid Earth 125 (5) e2019JB018992.
Sun, Y., Carrigan, C.R., 2014. Modeling noble gas transport and detection for the Comprehensive Nuclear-Test-Ban Treaty. Pure Appl. Geophys. 171 (3–5), 735–750.
Szatanik-Kloc, A., Szerement, J., Adamczuk, A., Józefaciuk, G., 2021. Effect of low zeolite doses on plants and soil physicochemical properties. Materials 14 (10), 2617.
Telfeyan, K., Ware, S.D., Reimus, P.W., Birdsell, K.H., 2018. Comparison of experimental methods for estimating matrix diffusion coefficients for contaminant transport modeling. J. Contam. Hydrol. 209, 51–60.
Veland, V.F., 2017. *Magnetic Resonance Imaging of Hydrate Phase Transitions in Sediments* (Master's Thesis. The University of Bergen.
Wohletz, K., Wolfsberg, A., Olson, A., Gable, C., 1999. Evaluating the effects of underground nuclear testing below the water table on groundwater and radionuclide migration in the tuff pile 1 region of Yucca flat: numerical simulations. In: EES–1 UGTA FY99 Report.
Xu, H., 2020. Probing nanopore structure and confined fluid behavior in shale matrix: a review on small-angle neutron scattering studies. Int. J. Coal Geol. 217, 103325.